

# Harvesting Sub-bandgap Photons via Upconversion for Perovskite Solar Cells

Roja Singh,<sup>#</sup> Eduard Madirov,<sup>#</sup> Dmitry Busko, Ihtez M. Hossain, Vasilii A. Konyushkin, Andrey N. Nakladov, Sergey V. Kuznetsov, Amjad Farooq, Saba Gharibzadeh, Ulrich W. Paetzold,<sup>\*</sup> Bryce S. Richards, and Andrey Turshatov<sup>\*</sup>

**ABSTRACT:** Lanthanide based upconversion (UC) allows harvesting sub bandgap near infrared photons in photovoltaics. In this work, we investigate UC in perovskite solar cells by implementing UC single crystal  $\text{BaF}_2:\text{Yb}^{3+}, \text{Er}^{3+}$  at the rear of the solar cell. Upon illumination with high intensity sub bandgap photons at 980 nm, the  $\text{BaF}_2:\text{Yb}^{3+}, \text{Er}^{3+}$  crystal emits upconverted photons in the spectral range between 520 and 700 nm. When tested under terrestrial sunlight representing one sun above the perovskite's bandgap and sub bandgap illumination at 980 nm, upconverted photons contribute a  $0.38 \text{ mA/cm}^2$  enhancement in the short circuit current density at lower intensity. The current enhancement scales non linearly with the incident intensity of sub bandgap illumination, and at higher intensity,  $2.09 \text{ mA/cm}^2$  enhancement in current was observed. Hence, our study shows that using a fluoride single crystal like  $\text{BaF}_2:\text{Yb}^{3+}, \text{Er}^{3+}$  for UC is a suitable method to extend the response of perovskite solar cells to near infrared illumination at 980 nm with a subsequent enhancement in current for very high incident intensity.

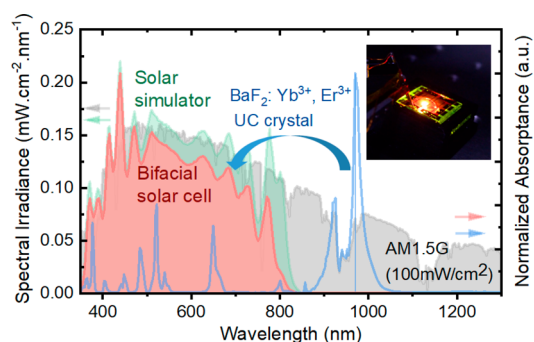
**KEYWORDS:** perovskite solar cells, sub bandgap transmission loss,  $\text{BaF}_2$  crystal, lanthanide, upconversion

## INTRODUCTION

Record power conversion efficiency (PCE) of perovskite solar cells (PSCs) recently surpassed 25% after just over one decade of research and development.<sup>1</sup> Enhancing the PCE further is a key measure to decrease the cost of electricity generated from perovskite photovoltaics (PV) and one strategy to achieve this is to utilize the solar spectrum more efficiently.<sup>2,3</sup> Of all the third generation PV concepts, the field of perovskite PV tandem devices – comprising a wide bandgap PSC combined with a low bandgap absorber, such as silicon – currently exhibits the record PCE.<sup>4,5</sup> Considering the PCE has surpassed that of record silicon single junction devices, these advances raise significant interest in research and industry.<sup>6</sup> The technology however still faces severe challenges in the device architecture related to the required current matching in the monolithic two terminal PSC<sup>7</sup> or parasitic absorption losses in multiterminal silicon perovskite tandem cells that require several transparent conductive oxides.<sup>8</sup> An alternative third generation PV concept is spectral conversion, which targets tailoring the incident solar spectrum such that it is more suitable for light harvesting by a solar cell with a single absorber.<sup>2,3,9,10</sup> There are two ways to realize this. On the one hand, a down conversion (DC) layer is used on top of the solar cell that reduces thermalization losses by generating two or more low energy photons from a single high energy photon.<sup>9,11,12</sup> On the other hand, an upconversion (UC)

layer can be implemented at the rear of a bifacial solar cell to minimize sub bandgap (SB) transmission losses by generating a single higher energy photon from the annihilation of two low energy photons.<sup>10,13,14</sup> In this way, the implementation of UC allows effectively extending the response of perovskite solar cells to the NIR range below the perovskite's bandgap.

A conventional upconverting (UC) material consists of an inorganic host and lanthanide dopant ions. Materials co doped with  $\text{Er}^{3+}$  and  $\text{Yb}^{3+}$  ions, in the form of nanocrystals, micro powders, and single crystals are a popular choice for upconversion application due to the ability to convert radiation around 1000 nm into the visible range. In the mid 90s,  $\text{Yb}^{3+}/\text{Er}^{3+}$  co doped UC phosphors were employed in GaAs PV devices,<sup>15</sup> while in 2005, singly doped  $\text{Er}^{3+}$  UC layers were applied on the rear of bifacial silicon solar cells.<sup>16</sup> Fischer *et al.* reported the record enhancement in  $J_{\text{SC}}$  of  $9.4 \text{ mA/cm}^2$  under concentrated sunlight (94 suns) by using  $\beta \text{ NaYF}_4:25\% \text{ Er}^{3+}$  micropowder embedded in a polymer on the rear side of a



bifacial silicon solar cell.<sup>17</sup> First studies on UC in PSCs can be broadly divided into three categories. First, UC nanocrystals were doped into different layers of the PSCs, namely, a hole transport layer (HTL),<sup>18</sup> the perovskite absorber layer itself,<sup>19</sup> and at the interfaces.<sup>20</sup> While doping improved the performance up to an optimal concentration, doping beyond the optimum proved to be disadvantageous as the nanocrystals now acted as recombination centers.<sup>18,20</sup> Second, triplet-triplet annihilation upconversion (TTA UC) was applied to PSCs.<sup>21,22</sup> Organic dyes, which are a part of the TTA upconverter, were embedded in polymeric sheets and placed behind a PSC as a UC layer.<sup>23</sup> Despite the promising enhancement in  $J_{SC}$ , the high excitation intensity (10 W/cm<sup>2</sup> or higher)<sup>25</sup> still required to upconvert near infrared (NIR) illumination into the visible range remains to be the main limitation on the use of TTA UC for PSCs. The third category uses UC inorganic materials in the form of single crystals or microcrystalline powders together with a PSC device stacked on top. These materials exhibit a much higher UC quantum yield compared to nanocrystals, since the latter have an increased number of surface defects that can cause additional luminescence quenching.<sup>24</sup> In addition, integration of nanoparticles into the various PSC layers limit the UC layer thickness to a few hundred nanometers.<sup>19–21</sup> Given the low absorption coefficient of lanthanide doped materials (typically  $\sim 13$  cm<sup>-1</sup> for 15 mol % Yb<sup>3+</sup> at 980 nm),<sup>25</sup> a 200 nm thick layer of densely packed UC nanoparticles should absorb a very small fraction of <0.03% of incident radiation at 980 nm. In contrast, a single crystal (or layer with dispersed UC microcrystals) can guarantee >90% absorption at 980 nm with a thickness of 1–2 mm. To date, there is only one study by Chen *et al.* that reported the use of LiYF<sub>4</sub>:Yb<sup>3+</sup>,Er<sup>3+</sup> single crystals placed on the front side of a PSC and demonstrated a 7.9% increase in PCE when excited with concentrated air mass 1.5 global (AM1.5G) sunlight at an intensity of 0.73 W/cm<sup>2</sup> (7–8 solar constants).<sup>26</sup> Hence, there is a lot of scope for exploring the excellent UC potential of these inorganic crystals for utilization of SB photons. Although the highest known upconversion quantum yield (UCQY) of 10.5%<sup>27</sup> is found in  $\beta$ -NaYF<sub>4</sub>:21.4 mol % Yb<sup>3+</sup>, 2.2 mol % Er<sup>3+</sup> under 980 nm excitation, the large single crystals of  $\beta$ -NaYF<sub>4</sub> are unknown. Only less efficient  $\alpha$ -NaYF<sub>4</sub> crystals can be easily grown using both Bridgman<sup>28</sup> and Czochralski methods.<sup>29</sup> Recently, UC materials that use MF<sub>2</sub> (M = Ca, Sr, Ba) hosts have been investigated. High UCQY upon 976 nm excitation was reported for SrF<sub>2</sub> (UCQY of 6.5%)<sup>25</sup> and BaF<sub>2</sub> crystals (UCQY of 10%)<sup>30</sup> doped with Er<sup>3+</sup> and Yb<sup>3+</sup>. It can be assumed that high UCQY observed in BaF<sub>2</sub> crystals is due to the lowest phonon energy in the series (CaF<sub>2</sub>, 320 cm<sup>-1</sup>;<sup>31</sup> SrF<sub>2</sub>, 284 cm<sup>-1</sup>;<sup>31</sup> and BaF<sub>2</sub>, 240 cm<sup>-130</sup>) that provides lower non-radiative losses. Thus, the BaF<sub>2</sub> crystal is chosen due to its prominent optical features such as high UCQY and brightness.

In this article, a BaF<sub>2</sub>:Yb<sup>3+</sup>, Er<sup>3+</sup> single crystal doped with 15% Yb<sup>3+</sup> and 2% Er<sup>3+</sup> is used for harvesting of the SB photons in a bifacial PSC. A brief description of the optical properties of the BaF<sub>2</sub>:Yb<sup>3+</sup>, Er<sup>3+</sup> single crystal along with an explanation of the UC process under NIR illumination is presented. Excitation of the combined PSC UC device is performed with SB illumination to confirm that the enhancement in  $J_{SC}$  indeed originates from UC of the SB photons. The possible effects of light soaking and temperature on the enhancement in  $J_{SC}$  are investigated, and the interrelation of UC and illumination intensity with SB photons is explored. Finally, a

conversion factor is calculated to determine the broad band (BB) illumination intensity (AM1.5G) that is equivalent to the intensity of the 980 nm laser used.

## EXPERIMENTAL DETAILS

**Fabrication of Solar Cells.** The bifacial solar cells with a layer stack of glass/ITO/SnO<sub>2</sub>/SAM C<sub>60</sub>/Cs<sub>0.17</sub>FA<sub>0.83</sub>PbI<sub>3</sub>/Spiro OMeTAD/MoO<sub>x</sub>/ITO/Au grids were prepared on 16 × 16 mm<sup>2</sup> patterned indium doped tin oxide (ITO) substrates with a sheet resistance of 15 Ω/□ (Luminescence Technology). The substrates were cleaned in an ultrasonic bath with acetone and isopropyl alcohol followed by oxygen plasma treatment for 3 min. A SnO<sub>2</sub> layer was deposited by spin coating using tin (IV) oxide 15% in H<sub>2</sub>O colloidal dispersion (Alfa Aesar). The colloidal SnO<sub>2</sub> was diluted with deionized water in the ratio 1:6.5 and spin coated at 4000 rpm followed by annealing at 250 °C for 30 min. Post annealing oxygen plasma treatment was done on the substrates for 1 min before further processing. A C<sub>60</sub> self-assembled monolayer (SAM) (Luminescence Technology) was used as passivation for the electron transport layer (ETL). 7.5 mg of C<sub>60</sub> SAM was mixed in 1 mL of 1,2-dichlorobenzene (Sigma Aldrich) and was left on a magnetic stirrer at 65 °C overnight for dissolving. The solution was filtered with a 0.2 μm polytetrafluoroethylene (PTFE) filter before it was spin coated on top of the SnO<sub>2</sub> at 4000 rpm and annealed at 120 °C for 5 min. Cs<sub>0.17</sub>FA<sub>0.83</sub>PbI<sub>3</sub> perovskite solution was prepared by dissolving 1.3 mmol of lead iodide in 1 mL of solvent mixture of *N,N*-dimethylformamide (Sigma Aldrich, CAS: 68 12 2):dimethylsulfoxide (Sigma Aldrich, CAS: 67 68 5) in a 4:1 ratio at 130 °C. In a separate glass vial, 1 mmol of formamidinium iodide (Dyesol, CAS: 879643 71 7) and 0.17 mmol of CsCl (Alfa Aesar, CAS: 7647 17 8) were weighed. The lead iodide solution was added to this vial after it was cooled down. The perovskite solution was spin coated using a two-step program of 1000–5000 rpm for 10–30 s. 120 μL of chlorobenzene (Sigma Aldrich, CAS: 108 90 7) was dropped on the center of the substrates at 15 s of the second step. The samples were annealed at 150 °C for 30 min in an inert atmosphere. 80 mg of spiro OMeTAD (Luminescence Technology) dissolved in 1 mL of chlorobenzene (Sigma Aldrich) doped with 17.5 μL of lithium bis(trifluoromethanesulfonyl)imide (Sigma Aldrich) and 28.5 μL of 4-*tert*-butylpyridine (Sigma Aldrich) was spin coated on top of the perovskite solution. The Li solution was made beforehand by dissolving 520 mg/mL lithium bis(trifluoromethanesulfonyl)imide in acetonitrile (Sigma Aldrich). The films were kept for aging for approximately 12 h in a dry box. 5 nm of MoO<sub>x</sub> (Sigma Aldrich) was thermally evaporated (Lesker) on top of the aged spiro OMeTAD before 160 nm of ITO was sputtered (Lesker) as a top contact. Finally, gold bands were evaporated on the edges for ease of probing.

**Characterization of Solar Cells.** The current density–voltage ( $J$ – $V$ ) characteristics and stabilized PCE of the bifacial devices were measured using a class AAA light emitting diode (LED) based solar simulator (Wavelabs, Sinus 70). The solar simulator provided a close match to the AM1.5G spectrum, as plotted in Figure S1. The calibration was achieved using a certified silicon reference solar cell (Fraunhofer) with a KG5 filter (Schott). A source meter (Keithley, 2450) was used to conduct  $J$ – $V$  measurements and maximum power point (MPP) tracking. Probes with gold pins (fabricated in house) were used to contact the cells for electrical measurements. The active area of the cell was 0.105 cm<sup>2</sup> and entire active area was completely illuminated during measurement. The scan rate used for measurements was 0.6 V/s. It takes  $\sim 5$  s to measure a bidirectional  $J$ – $V$  measurement (forward and reverse direction). A high scan rate was chosen in order to have minimum hysteresis in planar PSCs. Initial characterization of the fabricated PSCs showed high reproducibility. The statistics of the batch with 24 PSCs used for the experiment demonstrated similar device performance as depicted in Figure S2. The  $J$ – $V$  characteristics of the champion cell exhibited a PCE of 18% with a stabilized power output (SPO) of 17% under MPP tracking for 300 s, – see Figure S3. The temperature of PSCs during experiments with BB and SB illumination was determined using a thermal imager (Fluke, Ti400). For determining the temperature coefficient, the

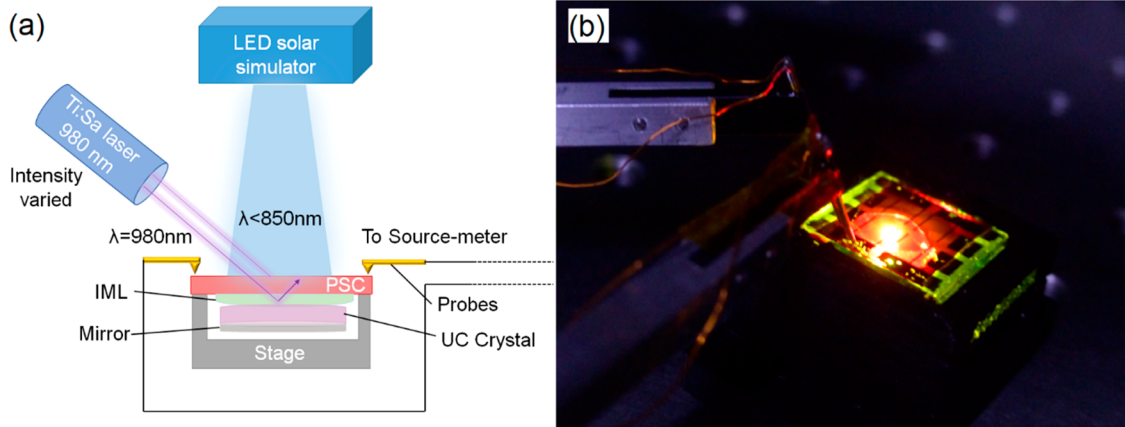


**Figure 1.** (a) Schematic representation of the experimental setup used for the measurement of enhancement in  $J_{SC}$  and the overall influence of UC on the PSC UC device. (b) Image of the bifacial cell and UC crystal under only 980 nm SB illumination at the intensity of  $4.5 \text{ W/cm}^2$ .

devices were heated from 25 to  $85 \text{ }^\circ\text{C}$  on a sample holder with a Peltier element. The devices were kept at a particular temperature for 2 min before performing  $J$ - $V$  measurements to ensure thermal equilibrium between the device and the holder. This range was chosen because under standard testing conditions (STC),<sup>32</sup> the devices have to be maintained at  $25 \text{ }^\circ\text{C}$  and for accelerated stability testing,<sup>32</sup>  $85 \text{ }^\circ\text{C}$  is the temperature of choice in the photovoltaic community.

External quantum efficiency (EQE) and ultraviolet–visible–near infrared (UV–Vis–NIR) spectra for PSCs were measured in a photovoltaic device characterization system (Bentham, PVE300). A monochromator was used to modulate the Xenon lamp. The chopper frequency of 905 Hz was used. The average  $J_{SC}$  of the PSC under  $100 \text{ mW/cm}^2$  of AM1.5G is  $\sim 21 \text{ mA/cm}^2$ , which is within 4% as calculated from the EQE measurement shown in Figure S4. Transmittance and reflectance of the device stacks were also measured using an integrating sphere in the same setup. Absorbance was calculated using the formula  $A = 1 - T - R$ , where  $T$  is the transmittance and  $R$  is the reflectance. The EQE for the PSC UC device was calculated from  $J_{SC}$ , which was measured using a source meter (Keithley, 2450) excited via a titanium:sapphire (Ti:Sa) continuous wave (CW) laser (M Squared Lasers Ltd., SolsTis).

**Synthesis of the UC Single Crystal.** The  $\text{BaF}_2:\text{Er}^{3+}, \text{Yb}^{3+}$  UC material was synthesized following the Bridgman method.<sup>28</sup> The nominal concentrations of  $\text{Yb}^{3+}$  and  $\text{Er}^{3+}$  are 15 and 2%, respectively. These values represent the amount of doping ions in the initial charge before the growing process. Meanwhile, the actual dopant concentration in the crystal of 11.98 and 1.86 mol % for  $\text{Yb}^{3+}$  and  $\text{Er}^{3+}$ , respectively, was determined with wavelength dispersive X ray fluorescence (WDXRF) spectroscopy (Bruker AXS, Pioneer S4).<sup>30</sup> The synthesis method produced the UC material in a cylindrical shape with a length of 5 cm. For the investigations in this work, a 1.7 mm thick disk was cut from the original bulk sample. This optimum thickness was determined based on a model that demonstrates that a thickness between 1 and 1.7 mm yields the highest numbers of UC photons, as detailed in the Supporting Information, Model to determine the optimum thickness of the UC single crystal (Figures S5–S9).

**Optical Characterization of the UC Single Crystal.** The detailed description of the optical setup used for the study of the optical properties of the UC single crystal can be found elsewhere.<sup>25,33</sup> Briefly, to measure the UC quantum yield – the ratio of the number of photons emitted via UC to the number absorbed at the excitation wavelength – the sample was placed in the middle of an integrating sphere (Labsphere,  $\text{Ø}15\text{cm}$ , 3P LPM 060 SL). It was excited with a 976 nm laser diode (Thorlabs, L980P200) mounted on a temperature controlled mount (Thorlabs, TCLDM9) and driven using a laser diode controller (Thorlabs, ITC4001). The excitation intensity was changed with a computer controlled filter wheel (Thorlabs, NDC 100C 2), and the excitation power was measured with a power

meter (Thorlabs, PM320E) using a fraction of laser intensity (4%) reflected off a glass wedge placed into the beam path. The whole optical system was calibrated using a calibration lamp (Ocean Optics, HL 3plus INT CAL EXT). The UC emission spectra were recorded using the setup for measurements of the UC quantum yield.

**Characterization of the PSC-UC Device.** A tunable Ti:Sa CW laser (M Squared Lasers Ltd., SolsTis) pumped by a 532 nm laser (Coherent, Verdi V18) was used as a source of 980 nm emission. A fraction of the beam reflected off a quartz wedge placed in the beam path was directed at a photodiode power sensor (Thorlabs, S122C) connected to a power meter (Thorlabs, PM100D) and used to control the laser intensity. This power measured was calibrated to the actual power reaching the sample. The size of the laser beam was measured with a camera based beam profiler (Thorlabs, BC106N, VIS/M). The device was placed in the same position as the crystal and an image was taken. It was assumed that the beam has an elliptical shape and the two axes of the ellipsoid were calculated from fitted Gauss functions as  $1/e^2$  width = 1.699 FWHM. A 100 cm focal length lens (Thorlabs) was additionally used to enhance the geometric concentration of the Ti:Sa laser.

The experimental setup used for the measurement of enhancement in  $J_{SC}$  and the overall influence of UC on the PSC are illustrated in Figure 1a. A holder was used to accommodate the bifacial PSC with the UC crystal at the rear. This combination of the PSC with the UC crystal is referred to as the PSC UC device. To ensure light coupling between the two and avoid unwanted reflections from surfaces, silicone immersion oil was used between the glass side of the PSC and the UC crystal as an index matching liquid (IML). The refractive index of the IML ( $n = 1.49$ )<sup>34</sup> is close to that of the UC crystal ( $n = 1.48$ )<sup>35</sup> at 980 nm. An LED based solar simulator was used to excite the samples. The solar simulator was programmed such that output wavelengths were chosen to match the AM1.5G spectrum in the range 350–850 nm. This was achieved by turning the channels at longer wavelengths ( $>850 \text{ nm}$ ) off. This precautionary measure was taken to ensure that the excitation in the SB range of  $>850 \text{ nm}$  comes only from the NIR bias light source (Ti:Sa laser) – even though the intensity of the NIR part of the spectrum provided by the solar simulator is low in comparison. The intensity of the solar simulator was  $\sim 70 \text{ mW/cm}^2$  throughout the experiment and is referred to as BB illumination. The wavelength of the illumination of the Ti:Sa laser was tuned to 980 nm as the  $\text{BaF}_2:15\%\text{Yb}^{3+}, 2\%\text{Er}^{3+}$  crystal exhibits its highest absorption coefficient at 974–980 nm (attributed to the transition  $\text{Yb}^{3+}:^2\text{F}_{7/2}$  to  $^2\text{F}_{5/2}$ ) – shown in Figure S1. In the experiments conducted within this work, the intensity of the NIR light source was varied and is referred to as the SB illumination. Continuous BB illumination and additionally cycled SB illumination at 980 nm ( $\sim 4.2 \text{ W/cm}^2$ ) having a period of 200 s and 50% duty cycle were used as an excitation source for spectral dependence and MPP tracking experiments. The stabilized power output (SPO) from

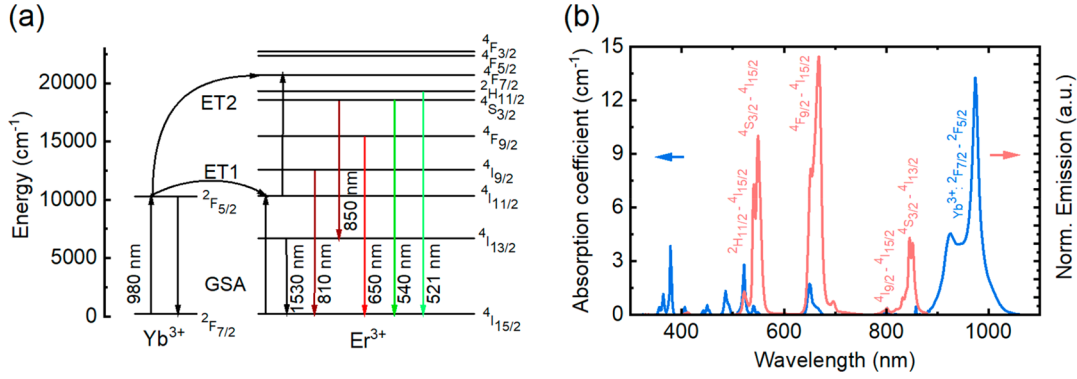


**Figure 2.** (a) Energy level diagrams of the  $\text{Er}^{3+}$  and  $\text{Yb}^{3+}$  ions along with the energy transfer (ET) UC mechanism. (b) Absorption coefficient and normalized emission spectra of the UC crystal (emission measured under 980 nm excitation).

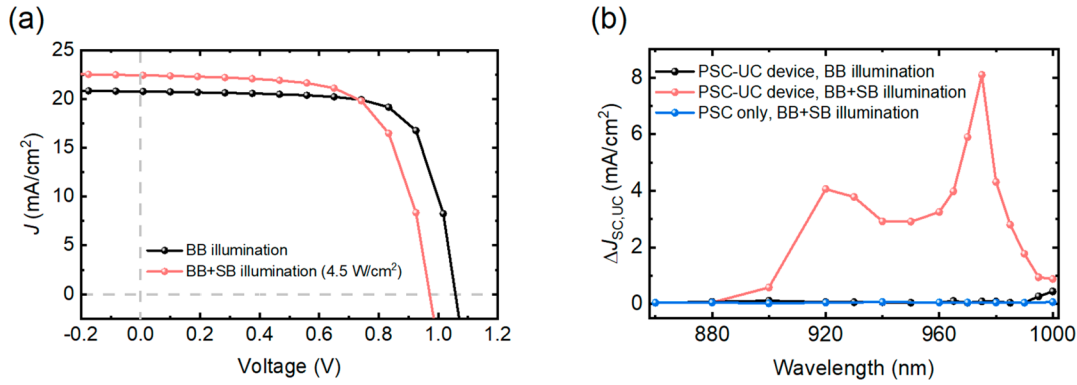


**Figure 3.** (a) Current density–voltage ( $J$ – $V$ ) characteristic of the PSC UC device excited with only BB illumination (black) and BB + SB illumination (red). Intensity at SB illumination was at  $4.5 \text{ W/cm}^2$ . (b) Spectral dependence of  $\Delta J_{\text{sc,UC}}$  measured from 860–1000 nm,  $\sim 4.2 \text{ W/cm}^2$  at different conditions: (i) PSC UC device and with only BB illumination (black), (ii) PSC UC device with BB + SB illumination (red), and (iii) PSC only with BB + SB illumination (blue).

MPP tracking was normalized to maximum power value. In our setup, since the BB + SB illumination was excited from the top, cooling of the PSC could only be implemented from the bottom of the PSC. However, due to the presence of the UC crystal (which acts as a thermal insulator) beneath the PSC, the cooling mechanism could not be applied. Convection cooling might also not be effective for such a highly concentrated source of illumination as the laser.<sup>36</sup> Therefore, the temperature of the PSC was not maintained to the STC of  $25^\circ\text{C}$ . The green and red emissions from the PSC upon illumination by NIR illumination are shown in Figure 1b.

## RESULTS

Here,  $\text{BaF}_2:\text{Yb}^{3+}, \text{Er}^{3+}$  is used as the UC material as it can be grown as a single crystal and possesses a low phonon energy ( $\sim 240 \text{ cm}^{-1}$ ).<sup>30</sup> The latter contributes to reduced non radiative losses and thus results in a high UC quantum yield.<sup>30</sup> The  $\text{Yb}^{3+}$  ion functions as a sensitizer and harvests light in the SB range (860–1080 nm). It then transfers the energy to the  $\text{Er}^{3+}$  ion that acts as an activator and emits the upconverted photons.<sup>37</sup> The co doping using  $\text{Yb}^{3+}$  and  $\text{Er}^{3+}$  ions is favorable for the UC process. This is due to the fact that  $\text{Yb}^{3+}$  exhibits a higher absorption cross section of the excited state ( $^2\text{F}_{5/2}$ ) compared to that of  $\text{Er}^{3+}$  state with similar energy ( $^4\text{I}_{11/2}$ ).<sup>38</sup> Besides this, the near resonant nature of these two levels allows an efficient energy transfer (ET) process from  $\text{Yb}^{3+}$  to  $\text{Er}^{3+}$  as shown in Figure 2a. The UC emission spectrum – displayed in Figure 2b – illustrates the multiple emission bands of  $\text{Er}^{3+}$ , all resulting from transitions from a range of excited states back to the ground state  $^4\text{I}_{15/2}$ . While the

emissions  $\geq 810 \text{ nm}$  will either be transmitted or reflected by the perovskite layer, the energy of the red and green emission exceeds the bandgap of the perovskite absorber. Hence, these photons can be absorbed by the perovskite layer and thereby contribute to the photocurrent generation.

The PSCs in focus of this study were prepared in a bifacial architecture, details of which were described earlier. The double cation  $\text{Cs}_{0.17}\text{FA}_{0.83}\text{PbI}_3$  perovskite layer exhibits a bandgap of  $1.57 \text{ eV}$ .<sup>39,40</sup> Thus, any photon with energy  $< 1.57 \text{ eV}$  ( $> 810 \text{ nm}$ ) cannot generate electron–hole pairs in the perovskite absorber. Among the various lead based perovskite, formamidinium lead iodide (FAPbI<sub>3</sub>) has the lowest bandgap of  $1.47 \text{ eV}$ .<sup>41</sup> FAPbI<sub>3</sub> is thermodynamically unstable in ambient temperature and degrades to its  $\delta$  FAPbI<sub>3</sub> phase.<sup>42</sup> A small amount of additives like cesium (Cs),<sup>40</sup> methyl ammonium (MA),<sup>43</sup> etc. can stabilize the phase to  $\alpha$  FAPbI<sub>3</sub> in ambient temperature, which is the photoactive phase. For this reason, we have used a small amount of Cs ( $\sim 17\%$ ) to stabilize the perovskite. However, such additives can cause a shift in the bandgap of the absorber. Considering the relatively higher stability at high temperature at the cost of an increased bandgap ( $1.57 \text{ eV}$ ),<sup>44</sup> CsFAPbI<sub>3</sub> was the absorber of choice. Effects of temperature on the performance of PSC have been discussed in further detail in the following section. We are also aware that other low bandgap perovskite absorbers like methylammonium lead iodide (MAPbI<sub>3</sub>) and Tin Lead (Sn Pb) perovskite exhibit lower bandgap than the absorber we have used; however, these materials have poor thermal

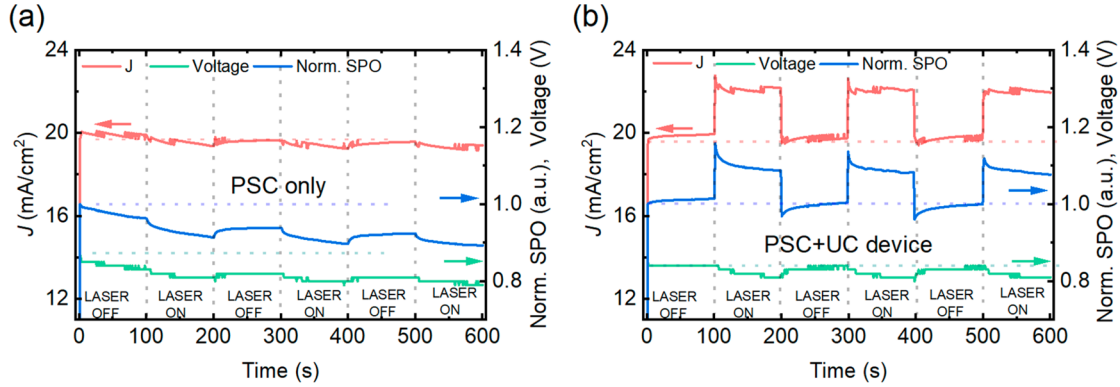


**Figure 4.** Current density (red), normalized stabilized power output (blue), and voltage (green) tracked for (a) the PSC only and (b) the PSC UC device near the maximum power point (MPP) over 600 s with continuous air mass 1.5 global (AM1.5G) illumination and additional cycled sub bandgap excitation at (980 nm, 4.2 W/cm<sup>2</sup>) having a period of 200 s and 50% duty cycle.

stability.<sup>45,46</sup> To realize the contribution of the photocurrent from photons with energy above the bandgap of the perovskite absorber and from the upconverted photons, a custom measurement setup was used in this study as illustrated in Figure 1a and described in detail in the Experimental Details section. At 980 nm, around 60% of the SB photons are transmitted through the bifacial perovskite solar cell – see transmission in Figure S10 – and subsequently absorbed by the UC crystal. When re emitted as higher energy photons by the UC crystal as depicted in the picture in Figure 1b and absorbed by the perovskite layer, they contribute to photocurrent generation in the PSC.

To obtain insight about the contributions of the upconverted photoemission to the photocurrent generation in the PSCs,  $J$ - $V$  measurements were performed under BB + SB illumination. The intensity of SB illumination was set to  $\sim 4.5$  W/cm<sup>2</sup>. A noticeable enhancement (red) in  $J_{SC}$ , as compared to only BB illumination (black), was observed in the PSC UC device as shown in Figure 3a. A maximum value of 22.4 mA/cm<sup>2</sup> was measured for the PSC UC device at 980 nm (4.5 W/cm<sup>2</sup>). To further comprehend the contribution of the spectral response in the increased  $J_{SC}$ , the excitation wavelength of the Ti:Sa laser was varied from 860 to 1000 nm and the photocurrent was measured. Absolute enhancement in  $J_{SC}$  due to UC ( $\Delta J_{SC,UC}$ ) was calculated – presented in Figure 3b – based on the following eq 1:

$$\Delta J_{SC,UC} = \frac{I_{SC(BB+SB \text{ illumination})} - I_{SC(BB \text{ illumination})}}{A_{spot}} \quad (1)$$

where  $I_{SC(BB+SB \text{ illumination})}$  is the short circuit current measured under BB + SB illumination,  $I_{SC(BB \text{ illumination})}$  is the short circuit current only under BB illumination, and  $A_{spot}$  is the size of the laser beam spot. The results indicated that the PSC UC device excited with both BB + SB illumination yields an increase in current density  $\Delta J_{SC,UC}$  if the SB illumination appears in the wavelength range 974–980 nm. This observation is well in line with the absorption spectra of the UC crystal as shown in Figure 2b and implies that the resultant increase in the  $J_{SC}$  originates from the UC crystal. External quantum efficiency measured from the  $J_{SC}$  showed that the maximum EQE ( $2.75 \times 10^{-2}\%$  at 975 nm, 4.2 W/cm<sup>2</sup>) contribution was below 1% for these PSC UC devices. The rather low enhancement in EQE is attributed mostly to the low UC quantum yield of BaF<sub>2</sub>:Yb<sup>3+</sup>, Er<sup>3+</sup> UC crystals of max.  $\sim 1\%$  at these intensities (refer to Figure S11). Furthermore, it must be taken into

account that there are additional reflection and parasitic absorption losses of these upconverted photons before they can be converted into charge carriers by the perovskite absorber. Nevertheless, the results indicate that if the UC quantum yield of the UC crystal can be increased, more SB photons can be harvested. The results presented in Figure 3a also show that along with the desired increase in  $J_{SC}$  with increasing excitation intensity of SB illumination, both the open circuit voltage ( $V_{OC}$ ) and the fill factor (FF) of the PSC decreased. This decrease could be due to the increased temperature of the PSC due to a prolonged exposure to the intense SB illumination.<sup>47,48</sup> An increase in temperature will reduce the built in voltage,<sup>49,50</sup> which subsequently increases the minority charge carrier recombination<sup>51,52</sup> and decreases the  $V_{OC}$ .<sup>53,54</sup> Furthermore, due to heat, the activation energy of the ions are reduced, which can lead to ion migration. During ion migration, ions accumulating at the perovskite/charge transport layer interface act as a barrier to the extraction of charge carriers and decrease the FF.<sup>55</sup> The BB + SB illumination at an intensity of 4.2 W/cm<sup>2</sup> raised the temperature of PSC to  $\sim 41$  °C (maximum of  $\sim 56$  °C and minimum of  $\sim 20$  °C) as shown in Figure S12a. The device temperature during the experiment was determined by using a thermal imager as mentioned above. A quantitative study of the effect of temperature on PSCs was performed to understand the detrimental effect of temperature. Detailed description of the experiment is provided in the Experimental Details section. The temperature coefficient of the PSC is presented in Figure S12b. The normalized values vs temperature depicts that  $V_{OC}$  and FF are two parameters that are highly influenced by the increment in temperature. The  $V_{OC}$  drops at a rate of  $-0.17$  rel.%/°C and FF decreases at  $-0.18$  rel.%/°C simultaneously, causing the PCE to have a drastic drop of  $-0.31$  rel.%/°C.  $J_{SC}$  however remains unaffected with the increase in temperature. At a temperature of  $\sim 41$  °C, the  $V_{OC}$  drop is approximately 0.97 V, which is in close comparison to the  $V_{OC}$  drop shown in Figure 3a.

Light soaking is a phenomenon where the PCE of the PV device is known to change as a function of time under constant illumination. As the samples were excited with BB and/or SB illumination continuously in the previous experiment, understanding the contribution of light soaking in the observed enhancement of  $\Delta J_{SC,UC}$  is necessary. To study the effect of light soaking, transient responses ( $J$ , SPO, Voltage) of the PSC UC device to SB illumination were investigated. The

PSC UC device was excited with BB illumination along with an additional cycled SB illumination as shown in Figure 4a. The result showed that for PSC only, the  $J$  remained constant during both the on and off cycles of the SB illumination. This indicated that the SB illumination does not affect the value of  $J$ . Although  $J$  was unchanged, the voltage was reduced during the on cycle, presumably due to additional heat that was generated in the cell. As a result, a decrease in the SPO was observed. As soon as the off cycle started, the SPO increased and stabilized close to its initial value. For the PSC UC device, a sudden increase was observed in the value of  $J$  as the SB illumination was switched on as shown in Figure 4b. Even though the voltage was reduced in a more gradual trend (as PSC only), during the on cycle, the increase in the  $J$  compensated for the losses. Hence, an overall increase in the SPO was observed. It should also be noted that during the on cycle with the PSC UC device,  $J$  remained steady, while a decay response for both the voltage and the SPO is observed. The drop in the voltage during this MPP tracking with BB + SB illumination is smaller than the drop observed in the  $J$ - $V$  measurement in Figure 3a. This is because in MPP conditions, the splitting of the quasi fermi level is reduced, resulting in a lower voltage. Furthermore, this transient response of the PSC in the SPO could be associated with ion migration in the perovskite layer with accumulation of the charge carriers at the perovskite/charge transport layer interface, as discussed above.

UC is a non linear process, which means that the quantum yield depends highly on the intensity of the incident photons.<sup>10</sup> To vary the intensity of SB illumination, the laser power was increased between 0.6 and 4.5 W/cm<sup>2</sup> while keeping the wavelength at 980 nm. The UC crystal showed the highest absorption at this wavelength. To achieve even higher intensity of the excitation, a lens was placed in the beam path such that it focused the laser beam on the crystal with a relatively smaller beam spot (see Figure S13). For the given UC crystal, the UC quantum yield is depicted in Figure S11. At low illumination intensity of about 0.6 W/cm<sup>2</sup>, a UC quantum yield of  $\phi_{UC} = 0.2\%$  is achieved. However, with increasing excitation intensity, the UC quantum yield increases steadily with values >1% at intensity exceeding 10 W/cm<sup>2</sup>.

The source of sub bandgap illumination is spectrally concentrated with a narrow linewidth. In order to estimate how concentrated a broadband spectrum such as AM1.5G was needed to get the same photon intensity in the NIR range and achieve the same  $\Delta J_{SC,UC}$ , a concentration factor ( $C$ ) was calculated. Equation S1 in the Supporting Information gives further details on  $C$ , which is followed from a previous work by Fischer *et al.*<sup>16,56</sup> It was approximated that a concentration of 197 times AM1.5G sunlight (from 860 nm to 1080 nm at 70 mW/cm<sup>2</sup>) would be necessary to achieve the same effect as 1 W/cm<sup>2</sup> of laser illumination at 980 nm. The lowest intensity of the CW laser that provided a measurable value of  $\Delta J_{SC,UC}$  (0.38 mA/cm<sup>2</sup>) was equivalent to 120 suns (0.6 W/cm<sup>2</sup>). A maximum of  $\Delta J_{SC,UC} = 2.09$  mA/cm<sup>2</sup> was measured at 880 suns (4.5 W/cm<sup>2</sup>) without using any focusing lens. By integrating optics into the system, the geometric concentration and the incident excitation can be increased. There are two options for placing this optics: (i) between the PSCs and the single crystal and (ii) between the light source and the solar cell. As shown in the experiments with silicon solar cells, although the optical element introduced between the solar cell and the UC layer did increase the quantum yield of the UC process, it also disrupted the collection of the UC emission by

the solar cell.<sup>56</sup> In another example, the wavefronts of both the excitation and emission fields were modulated with incorporation of dielectric microbeads. Due to the extremely short Rayleigh range and small absorption cross section of lanthanide materials, the fraction of light, efficiently upconverted, was very small and had a rather weak impact on the generated UC photon flux. In order to avoid unwanted absorption and maximize the external UC generation efficiency, the Rayleigh range of the focused radiation should correlate to the size of the UC material.<sup>57</sup> In our experiment, this range was about 3 mm. Hence, a lens of 100 cm focal length was introduced in between the SB illumination source and the solar cell. Such high concentrations of illumination might be of little significance in the field of PV, but this experiment helps to understand the trend of  $\Delta J_{SC,UC}$ . The results of the absolute enhancement as a function of the laser intensity is reported in Table 1. Figure 5 shows the relationship between  $\Delta J_{SC,UC}$  and intensity.

**Table 1. Enhancement in  $J_{SC}$  due to UC with Constant BB Illumination of 70 mW/cm<sup>2</sup> and Intensity Variation of SB Illumination**

optics condition	SB illumination power (mW)	SB illumination intensity (W/cm <sup>2</sup> )	solar concentration factor (suns)	$\Delta J_{SC,UC}$ (mA/cm <sup>2</sup> )
w/o lens	5	0.6 ± 0.08	120 ± 15	0.4 ± 0.35
	35	4.5 ± 0.56	880 ± 110	2.1 ± 0.13
with 100 cm lens	10	10.0 ± 0.19	2230 ± 37	4.0 ± 2.01
	35	38.8 ± 0.65	7650 ± 128	21.8 ± 1.59

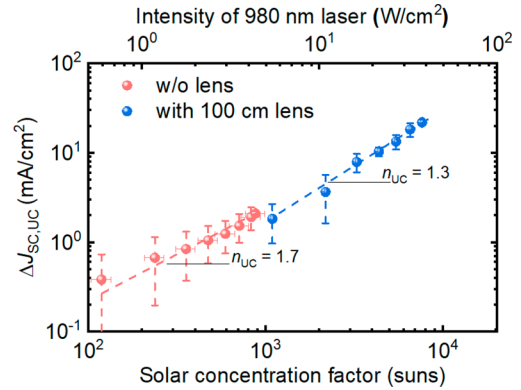


**Figure 5.** Enhancement in upconverted current density ( $\Delta J_{SC,UC}$ ) obtained for various solar concentrations. Red represents data without focusing and blue represents use of a lens of focal length 100 cm.

The measurement of  $\Delta J_{SC,UC}$  at lower intensity has higher deviation. This could arise from the inaccuracy with which the  $\Delta J_{SC,UC}$  or the area of the beam spot ( $A_{spot}$ ) was measured. Since an error in measurement of  $A_{spot}$  is more likely, a further discussion of how  $A_{spot}$  was measured is also presented in the Supporting Information. For measurements without the lens,  $A_{spot} = 0.15 \pm 0.01$  cm<sup>2</sup>. The obtained beam sizes and their deviation are presented in Table S1, alongside Figure S13, depicting  $A_{spot}$  for a laser source measured without and with a lens. The enhancement in  $\Delta J_{SC,UC}$ , compared to the reference, at 120 suns is only about  $\sim 0.4$  mA/cm<sup>2</sup>. However, significant enhancement up to  $\sim 2.1$  mA/cm<sup>2</sup> is demonstrated at 880 suns. It should be noted that introduction of the lens decreased the area of the beam spot ( $A_{spot} = 0.02 \pm 1.77 \times 10^{-4}$  cm<sup>2</sup>). A

maximum enhancement of  $\sim 21.8$  mA/cm<sup>2</sup> was achieved at 7650 suns. Measurements using a lower SB illumination power with the 100 cm lens (5.5 W/cm<sup>2</sup>, 1095 suns) have not been taken into consideration. Although the net intensity was much higher, the  $\Delta J_{SC,UC}$  measured was much lower than that at 4.5 W/cm<sup>2</sup> (measured w/o lens), the reason for which has been discussed previously.

## DISCUSSION

Further comparison with state of the art literature shows the potential of the device based on the PSC and BaF<sub>2</sub>:Yb<sup>3+</sup>, Er<sup>3+</sup> UC crystal for third generation PV. Recently, Kinoshita *et al.* reported the use of a TTA UC film at the rear of a PSC. Upon excitation with a diode laser (938 nm, 10 W/cm<sup>2</sup>), a  $\Delta J_{SC,UC}$  of 0.5 mA/cm<sup>2</sup> was observed.<sup>23</sup> While the approach is similar to that presented in this study, the novel BaF<sub>2</sub>:Yb<sup>3+</sup>, Er<sup>3+</sup> UC single crystal shows nearly 8 times stronger enhancement (4 mA/cm<sup>2</sup>) at the same intensity. This enhanced performance can be attributed to the higher absorption of the single crystal at 980 nm as compared to the TTA UC film used in the report by Kinoshita *et al.* Another important reference with this context is the work by Chen *et al.* with a remarkable enhancement of 7–8%.<sup>26</sup> However, it is unclear to the authors how such a high enhancement was achieved by placing the LiYF<sub>4</sub>:Yb<sup>3+</sup>, Er<sup>3+</sup> UC single crystal in front of the PSC, taking into account that placing the UC crystal in the path of the incident light may induce additional parasitic absorption losses. Parasitic absorption can arise as the UC crystal may absorb a certain part of the incident solar excitation in the range of 350–850 nm, reducing the amount of photons reaching the solar cell in the first place. It is also not clear from their manuscript how a light concentration of 7–8 solar constant was realized using only a solar simulator. Details of the type of laser used, filter implemented to achieve the stimulated sunlight (>800 nm), and how beam area was measured are also lacking. In essence, it was not possible to make direct comparison of LiYF<sub>4</sub>:Yb<sup>3+</sup>, Er<sup>3+</sup> and BaF<sub>2</sub>:Yb<sup>3+</sup>, Er<sup>3+</sup> single crystals applied for the PSC.

As lower  $J_{SC}$  enhancement was observed in our work compared to that of the LiYF<sub>4</sub>:Yb<sup>3+</sup>, Er<sup>3+</sup> single crystal, possible optical losses were examined in more detail. The intensity dependence of UC luminescence demonstrates power coefficient  $n_{UC} = 1.7$  at intensity >10 W/cm<sup>2</sup> as depicted in Figure S11 of the Supporting Information. However, as demonstrated in Figure 5,  $\Delta J_{SC,UC}$  increases with power coefficient  $n_{UC} = 1.3$  at similar intensity. The observed difference in the power coefficient suggested that there are additional loss mechanisms in the device compared to the freestanding crystal. A reflection loss of 4% can be expected for normal incidence from air on a surface with  $n > 1$  in the PSC only.<sup>58</sup> In the case of the PSC UC device, additional reflection loss can be expected between the UC crystal–air and air–PSC interface, if the PSC and UC crystal are not optically coupled. However, the use of IML in this work eliminated this additional loss. A significant portion of the incident excitation of  $\sim 26\%$  is lost through the escape cones.<sup>58</sup> Even implementing a back reflector, as done in this work, does not help curb this problem as the reflected light is lost from the front face.<sup>58</sup> Additionally, the PSC has  $\sim 30\%$  absorptance at 980 nm. The energy of the absorbed photons are dissipated only as heat. It has been previously discussed that heating of the device modifies its PV characteristics. Thus, the temperature negatively affected the performance of the PSC UC

device. In depth understanding of the effects of increased temperature and precautionary measures to be taken to avoid its detrimental effects is a topic of further research. Two questions remain yet unanswered. First, what is the most effective manner to properly utilize UC in PV. Second, considering that the size of single crystals is limited with the established synthesis techniques, what methods can be applied to effectively upscale such crystals for incorporation into large scale devices while maintaining their effectiveness. Fluoride materials in the form of large discs are possible to implement by means of optical ceramics production, as described in the review.<sup>59</sup> A recent review by Richards *et al.* indicates that several orders of magnitude increase in the generation rate is required before UC can begin to be an efficient process;<sup>60</sup> thus, taking advantage of nanophotonic structures,<sup>61</sup> plasmonics,<sup>62</sup> and concentrated light<sup>63</sup> all becomes interesting approaches.

## CONCLUSIONS

This work reports that the utilization of SB photons for photovoltaics is indeed possible via the use of a UC single crystal like BaF<sub>2</sub>:Yb<sup>3+</sup>, Er<sup>3+</sup>. The following conclusions can be drawn. First, upon irradiating the PSC UC device with BB + SB illumination, noticeable enhancement in  $J_{SC}$  as compared to BB illumination was observed. This confirms that the UC of SB photons with an UC material such as BaF<sub>2</sub>:Yb<sup>3+</sup>, Er<sup>3+</sup> is a viable way to increase the response of the PSC to NIR illumination. An enhancement of 0.38 mA/cm<sup>2</sup> as compared to the reference (without UC) was achieved at 0.6 W/cm<sup>2</sup> (equivalent to 120 suns). Second, the transient effect of light soaking was investigated by performing MPP tracking with cycling SB illumination at 4.2 W/cm<sup>2</sup> along with constant BB illumination. The PSC UC device showed a drastic increment in  $J$ , during SB illumination on cycle. However, in the PSC only, a detrimental effect of increased temperature was observed. This proved that  $\Delta J_{SC,UC}$  is not a time dependent, light soaking phenomenon. Third,  $\Delta J_{SC,UC}$  at lower intensity was not significant; however, upon an increment in intensity of SB illumination, a prominent enhancement of 2.09 mA/cm<sup>2</sup> was observed at 4.5 W/cm<sup>2</sup> (equivalent to 880 suns). Different losses and an increase in temperature can limit the  $\Delta J_{SC,UC}$ . However, by implementing methods to minimize the losses or by preventing the increment in temperature, one could also prevent these adverse effects. It would also help prevent increased dark saturation current and ion accumulation in the solar cell. Synthesis of more efficient UC material, development of advanced synthesis techniques, and fabrication of devices more suited for such applications can make the future prospects of UC crystals more promising in the context of SB energy harvesting.

## AUTHOR INFORMATION

### Corresponding Authors

Ulrich W. Paetzold – Institute of Microstructure Technology, Karlsruhe Institute of Technology, Eggenstein Leopoldshafen 76344, Germany; Light Technology Institute, Karlsruhe

Institute of Technology, Karlsruhe 76131, Germany;

• [orcid.org/0000 0002 1557 8361](https://orcid.org/0000-0002-1557-8361);

Email: [ulrich.paetzold@kit.edu](mailto:ulrich.paetzold@kit.edu)

**Andrey Turshatov** – Institute of Microstructure Technology, Karlsruhe Institute of Technology, Eggenstein Leopoldshafen 76344, Germany; • [orcid.org/0000 0002 8004 098X](https://orcid.org/0000-0002-8004-098X);  
Email: [andrey.turshatov@kit.edu](mailto:andrey.turshatov@kit.edu)

## Authors

**Roja Singh** – Institute of Microstructure Technology, Karlsruhe Institute of Technology, Eggenstein Leopoldshafen 76344, Germany; Light Technology Institute, Karlsruhe Institute of Technology, Karlsruhe 76131, Germany; • [orcid.org/0000 0002 2202 3612](https://orcid.org/0000-0002-2202-3612)

**Eduard Madirov** – Institute of Microstructure Technology, Karlsruhe Institute of Technology, Eggenstein Leopoldshafen 76344, Germany; Kazan Federal University, Kazan 420008, Russia

**Dmitry Busko** – Institute of Microstructure Technology, Karlsruhe Institute of Technology, Eggenstein Leopoldshafen 76344, Germany

**Ihtezaz M. Hossain** – Institute of Microstructure Technology, Karlsruhe Institute of Technology, Eggenstein Leopoldshafen 76344, Germany; Light Technology Institute, Karlsruhe Institute of Technology, Karlsruhe 76131, Germany; • [orcid.org/0000 0001 6533 1757](https://orcid.org/0000-0001-6533-1757)

**Vasilii A. Konyushkin** – Prokhorov General Physics Institute of the Russian Academy of Sciences, Moscow 119991, Russia

**Andrey N. Nakladov** – Prokhorov General Physics Institute of the Russian Academy of Sciences, Moscow 119991, Russia

**Sergey V. Kuznetsov** – Prokhorov General Physics Institute of the Russian Academy of Sciences, Moscow 119991, Russia

**Amjad Farooq** – Institute of Microstructure Technology, Karlsruhe Institute of Technology, Eggenstein Leopoldshafen 76344, Germany; Light Technology Institute, Karlsruhe Institute of Technology, Karlsruhe 76131, Germany; Institute for Materials Science and Center for Nanointegration Duisburg Essen (CENIDE), University of Duisburg Essen, Essen 45141, Germany

**Saba Gharibzadeh** – Institute of Microstructure Technology, Karlsruhe Institute of Technology, Eggenstein Leopoldshafen 76344, Germany; Light Technology Institute, Karlsruhe Institute of Technology, Karlsruhe 76131, Germany

**Bryce S. Richards** – Institute of Microstructure Technology, Karlsruhe Institute of Technology, Eggenstein Leopoldshafen 76344, Germany; Light Technology Institute, Karlsruhe Institute of Technology, Karlsruhe 76131, Germany; • [orcid.org/0000 0001 5469 048X](https://orcid.org/0000-0001-5469-048X)

## Author Contributions

#R.S. and E.M. have contributed equally to this work. U.W.P. and A.T. conceived the idea; A.F. and D.B. performed initial investigation; R.S. fabricated and characterized the solar cells; S.G. developed the double cation perovskite, and I.H. developed the semi-transparent ITO top contact; V.A.K., A.N.N., and S.V.K. synthesized the  $\text{BaF}_2:\text{Yb}^{3+}, \text{Er}^{3+}$  UC single crystal. E.M. characterized the  $\text{BaF}_2:\text{Yb}^{3+}, \text{Er}^{3+}$  UC single crystal. R.S. and E.M. performed experimentation involving the  $\text{BaF}_2:\text{Yb}^{3+}, \text{Er}^{3+}$  UC single crystal and solar cell. R.S. wrote the manuscript. B.S.R. provided extensive guidance on the measurement approach of combining UC materials with the

solar cells as well as developing a clear story for the manuscript. U.W.P. and A.T. supervised the project. All authors have given approval to the final version of the manuscript.

## Funding

The financial support of (i) German Federal Ministry for Economic Affairs and Energy (CAPITANO, funding code 03EE1038B); (ii) the Initiating and Networking funding of the Helmholtz Association (HYIG of U.W.P., funding code VH NG1148); (iii) the Materials and Technologies for the Energy Transition Research Program is acknowledged. Part of the reported study was also funded by RFBR (project number 21 53 12017 for S.V.K., V.A.K., and A.N.N.) and DFG (project number TU 487/8 1 for A.T. and B.S.R.). B.S.R. acknowledges the financial support provided by the Helmholtz Association: (i) a Recruitment Initiative Fellowship for B. S. R.; (ii) the funding of chemical synthesis equipment from the Helmholtz Materials Energy Foundry (HEMF); and (iii) the Research Field Energy – Program Materials and Technologies for the Energy Transition – Topic 1 Photovoltaics”. E.I.M. acknowledges the scholarship of the President of the Russian Federation.

## Notes

The authors declare no competing financial interest.

## ACKNOWLEDGMENTS

Special thanks are given to Paul Fassel for his support with the concentration factor analysis and Fabian Schackmar for his help with the instrumentation.

## REFERENCES

- (1) NREL Best Research Cell Efficiency Chart. [https://www.nrel.gov/pv/cell\\_efficiency.html](https://www.nrel.gov/pv/cell_efficiency.html) (accessed Sept 29, 2021).
- (2) Green, M. A. *Third Generation Photovoltaics: Advanced Solar Energy Conversion*; Springer: Berlin Heidelberg, 2003.
- (3) Green, M. A. Third Generation Photovoltaics: Ultra High Conversion Efficiency at Low Cost. *Prog. Photovolt.* **2001**, *9*, 123–135.
- (4) Green, M.; Dunlop, E.; Hohl Ebinger, J.; Yoshita, M.; Kopidakis, N.; Hao, X. Solar Cell Efficiency Tables (Version 57). *Prog. Photovolt.* **2021**, *29*, 3–15.
- (5) Al Ashouri, A.; Köhnen, E.; Li, B.; Magomedov, A.; Hempel, H.; Caprioglio, P.; Márquez, J. A.; Vilches, A. B. M.; Kasparavicius, E.; Smith, J. A.; Phung, N.; Menzel, D.; Grischek, M.; Kegelmann, L.; Skroblin, D.; Gollwitzer, C.; Malinauskas, T.; Jošt, M.; Matič, G.; Rech, B.; Schlatmann, R.; Topič, M.; Korte, L.; Abate, A.; Stannowski, B.; Neher, D.; Stolterfoht, M.; Unold, T.; Getautis, V.; Albrecht, S. Monolithic Perovskite/Silicon Tandem Solar Cell with >29% Efficiency by Enhanced Hole Extraction. *Science* **2020**, *370*, 1300–1309.
- (6) Sofia, S. E.; Wang, H.; Bruno, A.; Cruz Campa, J. L.; Buonassisi, T.; Peters, I. M. Roadmap for Cost Effective, Commercially Viable Perovskite Silicon Tandems for the Current and Future PV Market. *Sustainable Energy Fuels* **2020**, *4*, 852–862.
- (7) Brown, A. S.; Green, M. A. Limiting Efficiency for Current Constrained Two Terminal Tandem Cell Stacks. *Prog. Photovolt.* **2002**, *10*, 299–307.
- (8) Jacobs, D. A.; Langenhorst, M.; Sahli, F.; Richards, B. S.; White, T. P.; Ballif, C.; Catchpole, K. R.; Paetzold, U. W. Light Management: A Key Concept in High Efficiency Perovskite/Silicon Tandem Photovoltaics. *J. Phys. Chem. Lett.* **2019**, 3159–3170.
- (9) Trupke, T.; Green, M. A.; Würfel, P. Improving Solar Cell Efficiencies by Down Conversion of High Energy Photons. *J. Appl. Phys.* **2002**, *92*, 1668–1674.

- (10) Shalav, A.; Richards, B. S.; Green, M. A. Luminescent Layers for Enhanced Silicon Solar Cell Performance: Up Conversion. *Sol. Energy Mater. Sol. Cells* **2007**, *91*, 829–842.
- (11) Richards, B. S. Luminescent Layers for Enhanced Silicon Solar Cell Performance: Down Conversion. *Sol. Energy Mater. Sol. Cells* **2006**, *90*, 1189–1207.
- (12) Kroupa, D. M.; Roh, J. Y.; Milstein, T. J.; Creutz, S. E.; Gamelin, D. R. Quantum Cutting Ytterbium Doped CsPb(Cl<sub>1-x</sub>Br<sub>x</sub>)<sub>3</sub> Perovskite Thin Films with Photoluminescence Quantum Yields over 190%. *ACS Energy Lett.* **2018**, *3*, 2390–2395.
- (13) Trupke, T.; Green, M. A.; Würfel, P. Improving Solar Cell Efficiencies by Up Conversion of Sub Band Gap Light. *J. Appl. Phys.* **2002**, *92*, 4117–4122.
- (14) Richards, B. S. Enhancing the Performance of Silicon Solar Cells via the Application of Passive Luminescence Conversion Layers. *Sol. Energy Mater. Sol. Cells* **2006**, *90*, 2329–2337.
- (15) Gibart, P.; Auzel, F.; Guillaume, J. C.; Zahraman, K. Below Band Gap IR Response of Substrate Free GaAs Solar Cells Using Two Photon up Conversion. *Jpn. J. Appl. Phys.* **1996**, *35*, 4401–4402.
- (16) Shalav, A.; Richards, B. S.; Trupke, T.; Krämer, K. W.; Güdel, H. U. Application of NaYF<sub>4</sub>:Er<sup>3+</sup> up Converting Phosphors for Enhanced near Infrared Silicon Solar Cell Response. *Appl. Phys. Lett.* **2005**, *86*, No. 013505.
- (17) Fischer, S.; Ivaturi, A.; Jakob, P.; Krämer, K. W.; Martin Rodriguez, R.; Meijerink, A.; Richards, B.; Goldschmidt, J. C. Upconversion Solar Cell Measurements under Real Sunlight. *Opt. Mater.* **2018**, *84*, 389–395.
- (18) Deng, X.; Zhang, C.; Zheng, J.; Zhou, X.; Yu, M.; Chen, X.; Huang, S. Highly Bright Li(Gd,Y)F<sub>4</sub>:Yb,Er Upconverting Nanocrystals Incorporated Hole Transport Layer for Efficient Perovskite Solar Cells. *Appl. Surf. Sci.* **2019**, *485*, 332–341.
- (19) Lai, X.; Li, X.; Lv, X.; Zheng, Y. Z.; Meng, F.; Tao, X. Broadband Dye Sensitized Upconverting Nanocrystals Enabled near Infrared Planar Perovskite Solar Cells. *J. Power Sources* **2017**, *372*, 125–133.
- (20) Schoenauer Sebag, M.; Hu, Z.; De Oliveira Lima, K.; Xiang, H.; Gredin, P.; Mortier, M.; Billot, L.; Aigouy, L.; Chen, Z. Microscopic Evidence of Upconversion Induced Near Infrared Light Harvest in Hybrid Perovskite Solar Cells. *ACS Appl. Energy Mater.* **2018**, *1*, 3537–3543.
- (21) Monguzzi, A.; Mezyk, J.; Scotognella, F.; Tubino, R.; Meinardi, F. Upconversion Induced Fluorescence in Multicomponent Systems: Steady State Excitation Power Threshold. *Phys. Rev. B* **2008**, *78*, 195112.
- (22) Balushev, S.; Miteva, T.; Yakutkin, V.; Nelles, G.; Yasuda, A.; Wegner, G. Up Conversion Fluorescence: Noncoherent Excitation by Sunlight. *Phys. Rev. Lett.* **2006**, *97*, 143903.
- (23) Kinoshita, M.; Sasaki, Y.; Amemori, S.; Harada, N.; Hu, Z.; Liu, Z.; Ono, L. K.; Qi, Y.; Yanai, N.; Kimizuka, N. Photon Upconverting Solid Films with Improved Efficiency for Endowing Perovskite Solar Cells with Near Infrared Sensitivity. *ChemPhotoChem* **2020**, *4*, 5271–5278.
- (24) Boyer, J. C.; van Veggel, F. C. J. M. Absolute Quantum Yield Measurements of Colloidal NaYF<sub>4</sub>:Er<sup>3+</sup>, Yb<sup>3+</sup> Upconverting Nanoparticles. *Nanoscale* **2010**, *2*, 1417–1419.
- (25) Saleta Reig, D.; Grauel, B.; Konyushkin, V. A.; Nakladov, A. N.; Fedorov, P. P.; Busko, D.; Howard, I. A.; Richards, B. S.; Resch Genger, U.; Kuznetsov, S. V.; Turshatov, A.; Würth, C. Upconversion Properties of SrF<sub>2</sub>:Yb<sup>3+</sup>,Er<sup>3+</sup> Single Crystals. *J. Mater. Chem. C* **2020**, *8*, 4093–4101.
- (26) Chen, X.; Xu, W.; Song, H.; Chen, C.; Xia, H.; Zhu, Y.; Zhou, D.; Cui, S.; Dai, Q.; Zhang, J. Highly Efficient LiYF<sub>4</sub>:Yb<sup>3+</sup>, Er<sup>3+</sup> Upconversion Single Crystal under Solar Cell Spectrum Excitation and Photovoltaic Application. *ACS Appl. Mater. Interfaces* **2016**, *8*, 9071–9079.
- (27) Kaiser, M.; Würth, C.; Kraft, M.; Hyppänen, I.; Soukka, T.; Resch Genger, U. Power Dependent Upconversion Quantum Yield of NaYF<sub>4</sub>:Yb<sup>3+</sup>,Er<sup>3+</sup> Nano and Micrometer Sized Particles – Measurements and Simulations. *Nanoscale* **2017**, *9*, 10051–10058.
- (28) Yang, S.; Xia, H.; Jiang, Y.; Zhang, J.; Shi, Y.; Gu, X.; Zhang, J.; Zhang, Y.; Jiang, H.; Chen, B. Tm<sup>3+</sup> Doped  $\alpha$ -NaYF<sub>4</sub> Single Crystal for 2 mm Laser Application. *J. Alloys Compd.* **2015**, *643*, 1–6.
- (29) Cassanho, A.; Knowles, D.; Jenssen, H. P. Optical Properties of Nd:NaYF<sub>4</sub> and Ho:NaYF<sub>4</sub>. *Tunable Solid State Lasers* **1989**, 139–145.
- (30) Madirov, E. I.; Konyushkin, V. A.; Nakladov, A. N.; Fedorov, P. P.; Bergfeldt, T.; Busko, D.; Howard, I. A.; Richards, B. S.; Kuznetsov, S. V.; Turshatov, A. An Up Conversion Luminophore with High Quantum Yield and Brightness Based on BaF<sub>2</sub>:Yb<sup>3+</sup>,Er<sup>3+</sup> Single Crystals. *J. Mater. Chem. C* **2021**, *9*, 3493–3503.
- (31) Richman, I. Longitudinal Optical Phonons in CaF<sub>2</sub>, SrF<sub>2</sub>, and BaF<sub>2</sub>. *J. Chem. Phys.* **2004**, *41*, 2836.
- (32) Khenkin, M. V.; Katz, E. A.; Abate, A.; Bardizza, G.; Berry, J. J.; Brabec, C.; Brunetti, F.; Bulović, V.; Burlingame, Q.; Di Carlo, A.; Cheacharoen, R.; Cheng, Y. B.; Colmann, A.; Cros, S.; Domanski, K.; Duszka, M.; Fell, C. J.; Forrest, S. R.; Galagan, Y.; Di Girolamo, D.; Grätzel, M.; Hagfeldt, A.; von Hauff, E.; Hoppe, H.; Kettle, J.; Köbler, H.; Leite, M. S.; Liu, S.; Loo, Y. L.; Luther, J. M.; Ma, C. Q.; Madsen, M.; Manceau, M.; Matheron, M.; McGehee, M.; Meitzner, R.; Nazeeruddin, M. K.; Nogueira, A. F.; Odabaşı, Ç.; Osherov, A.; Park, N. G.; Reese, M. O.; De Rossi, F.; Saliba, M.; Schubert, U. S.; Snaith, H. J.; Stranks, S. D.; Tress, W.; Troshin, P. A.; Turkovic, V.; Veenstra, S.; Visoly Fisher, I.; Walsh, A.; Watson, T.; Xie, H.; Yildirim, R.; Zakeeruddin, S. M.; Zhu, K.; Lira Cantu, M. Consensus Statement for Stability Assessment and Reporting for Perovskite Photovoltaics Based on ISOS Procedures. *Nat. Energy* **2020**, *5*, 35–49.
- (33) Joseph, R. E.; Jiménez, C.; Hudry, D.; Gao, G.; Busko, D.; Biner, D.; Turshatov, A.; Krämer, K.; Richards, B. S.; Howard, I. A. Critical Power Density: A Metric to Compare the Excitation Power Density Dependence of Photon Upconversion in Different Inorganic Host Materials. *J. Phys. Chem. A* **2019**, *123*, 6799–6811.
- (34) Stöhr, M.; Roth, K.; Jähne, B. Measurement of 3D Pore Scale Flow in Index Matched Porous Media. *Exp. Fluids* **2003**, *35*, 159–166.
- (35) Malitson, I. H. Refractive Properties of Barium Fluoride. *J. Opt. Soc. Am.* **1964**, *54*, 628.
- (36) Ghazy, A.; Safdar, M.; Lastusaari, M.; Aho, A.; Tukiainen, A.; Savin, H.; Guina, M.; Karppinen, M. Luminescent (Er,Ho)<sub>2</sub>O<sub>3</sub> Thin Films by ALD to Enhance the Performance of Silicon Solar Cells. *Sol. Energy Mater. Sol. Cells* **2021**, *219*, 110787.
- (37) Menyuk, N.; Dwight, K.; Pierce, J. W. NaYF<sub>4</sub>:Yb,Er—an Efficient Upconversion Phosphor. *Appl. Phys. Lett.* **1972**, *21*, 159–161.
- (38) Suyver, J. F.; Grimm, J.; Krämer, K. W.; Güdel, H. U. Highly Efficient Near Infrared to Visible up Conversion Process in NaYF<sub>4</sub>:Er<sup>3+</sup>,Yb<sup>3+</sup>. *J. Lumin.* **2005**, *114*, 53–59.
- (39) Schultes, M.; Helder, T.; Ahlswede, E.; Aygüler, M. F.; Jackson, P.; Paetel, S.; Schwenzer, J. A.; Hossain, I. M.; Paetzold, U. W.; Powalla, M. Sputtered Transparent Electrodes (IO:H and IZO) with Low Parasitic Near Infrared Absorption for Perovskite Cu(In,Ga)Se<sub>2</sub> Tandem Solar Cells. *ACS Appl. Energy Mater.* **2019**, *2*, 7823–7831.
- (40) Gharibzadeh, S.; Abdollahi Nejand, B.; Jakoby, M.; Abzieher, T.; Hauschild, D.; Moghadamzadeh, S.; Schwenzer, J. A.; Brenner, P.; Schmäger, R.; Haghighirad, A. A.; Weinhardt, L.; Lemmer, U.; Richards, B. S.; Howard, I. A.; Paetzold, U. W. Record Open Circuit Voltage Wide Bandgap Perovskite Solar Cells Utilizing 2D/3D Perovskite Heterostructure. *Adv. Energy Mater.* **2019**, *9*, 1803699.
- (41) Masi, S.; Gualdrón Reyes, A. F.; Mora Seró, I. Stabilization of Black Perovskite Phase in FAPbI<sub>3</sub> and CsPbI<sub>3</sub>. *ACS Energy Lett.* **2020**, *5*, 1974–1985.
- (42) Ma, F.; Li, J.; Li, W.; Lin, N.; Wang, L.; Qiao, J. Stable  $\alpha/\delta$  Phase Junction of Formamidinium Lead Iodide Perovskites for Enhanced near Infrared Emission. *Chem. Sci.* **2017**, *8*, 800–805.
- (43) Binek, A.; Hanusch, F. C.; Docampo, P.; Bein, T. Stabilization of the Trigonal High Temperature Phase of Formamidinium Lead Iodide. *J. Phys. Chem. Lett.* **2015**, *6*, 1249–1253.
- (44) Li, Z.; Yang, M.; Park, J. S.; Wei, S. H.; Berry, J. J.; Zhu, K. Stabilizing Perovskite Structures by Tuning Tolerance Factor:

Formation of Formamidinium and Cesium Lead Iodide Solid State Alloys. *Chem. Mater.* **2016**, *28*, 284–292.

(45) Conings, B.; Drijkoningen, J.; Gauquelin, N.; Babayigit, A.; D'Haen, J.; D'Olieslaeger, L.; Ethirajan, A.; Verbeeck, J.; Manca, J.; Mosconi, E.; De Angelis, F.; Boyen, H. G. Intrinsic Thermal Instability of Methylammonium Lead Trihalide Perovskite. *Adv. Energy Mater.* **2015**, *5*, 1500477.

(46) Leijtens, T.; Prasanna, R.; Bush, K. A.; Eperon, G. E.; Raiford, J. A.; Gold Parker, A.; Wolf, E. J.; Swifter, S. A.; Boyd, C. C.; Wang, H. P.; Toney, M. F.; Bent, S. F.; McGehee, M. D. Tin Lead Halide Perovskites with Improved Thermal and Air Stability for Efficient All Perovskite Tandem Solar Cells. *Sustainable Energy Fuels* **2018**, *2*, 2450–2459.

(47) Zheng, X.; Chen, B.; Yang, M.; Wu, C.; Orlor, B.; Moore, R. B.; Zhu, K.; Priya, S. The Controlling Mechanism for Potential Loss in  $\text{CH}_3\text{NH}_3\text{PbBr}_3$  Hybrid Solar Cells. *ACS Energy Lett.* **2016**, *1*, 424–430.

(48) Shao, S.; Liu, J.; Fang, H. H.; Qiu, L.; ten Brink, G. H.; Hummelen, J. C.; Koster, L. J. A.; Loi, M. A. Efficient Perovskite Solar Cells over a Broad Temperature Window: The Role of the Charge Carrier Extraction. *Adv. Energy Mater.* **2017**, *7*, 1701305.

(49) Cao, R.; Xu, F.; Zhu, J.; Ge, S.; Wang, W.; Xu, H.; Xu, R.; Wu, Y.; Ma, Z.; Hong, F.; Jiang, Z. Unveiling the Low Temperature Pseudodegradation of Photovoltaic Performance in Planar Perovskite Solar Cell by Optoelectronic Observation. *Adv. Energy Mater.* **2016**, *6*, 1600814.

(50) Labram, J. G.; Fabini, D. H.; Perry, E. E.; Lehner, A. J.; Wang, H.; Claudell, A. M.; Wu, G.; Evans, H.; Buck, D.; Cotta, R.; Echegoyen, L.; Wudl, F.; Seshadri, R.; Chabinyc, M. L. Temperature Dependent Polarization in Field Effect Transport and Photovoltaic Measurements of Methylammonium Lead Iodide. *J. Phys. Chem. Lett.* **2015**, *6*, 3565–3571.

(51) Meloni, S.; Moehl, T.; Tress, W.; Franckevičius, M.; Saliba, M.; Lee, Y. H.; Gao, P.; Nazeeruddin, M. K.; Zakeeruddin, S. M.; Rothlisberger, U.; Graetzel, M. Ionic Polarization Induced Current Voltage Hysteresis in  $\text{CH}_3\text{NH}_3\text{PbX}_3$  Perovskite Solar Cells. *Nat. Commun.* **2016**, *7*, 1–19.

(52) Kim, S.; Bae, S.; Lee, S. W.; Cho, K.; Lee, K. D.; Kim, H.; Park, S.; Kwon, G.; Ahn, S. W.; Lee, H. M.; Kang, Y.; Lee, H. S.; Kim, D. Relationship between Ion Migration and Interfacial Degradation of  $\text{CH}_3\text{NH}_3\text{PbI}_3$  Perovskite Solar Cells under Thermal Conditions. *Sci. Rep.* **2017**, *1*, 1200.

(53) Green, M. A. General Temperature Dependence of Solar Cell Performance and Implications for Device Modelling. *Prog. Photovolt.* **2003**, *11*, 333–340.

(54) Singh, P.; Ravindra, N. M. Temperature Dependence of Solar Cell Performance—an Analysis. *Sol. Energy Mater. Sol. Cells* **2012**, *101*, 36–45.

(55) Bartesaghi, D.; del Carmen Pérez, I.; Kniepert, J.; Roland, S.; Turbiez, M.; Neher, D.; Koster, L. J. A. Competition between Recombination and Extraction of Free Charges Determines the Fill Factor of Organic Solar Cells. *Nat. Commun.* **2015**, *6*, 7083.

(56) Arnaoutakis, G. E.; Marques Hueso, J.; Ivaturi, A.; Fischer, S.; Goldschmidt, J. C.; Krämer, K. W.; Richards, B. S. Enhanced Energy Conversion of Up Conversion Solar Cells by the Integration of Compound Parabolic Concentrating Optics. *Sol. Energy Mater. Sol. Cells* **2015**, *140*, 217–223.

(57) Liang, L.; Teh, D. B. L.; Dinh, N. D.; Chen, W.; Chen, Q.; Wu, Y.; Chowdhury, S.; Yamanaka, A.; Sum, T. C.; Chen, C. H.; Thakor, N. V.; All, A. H.; Liu, X. Upconversion Amplification through Dielectric Superlensing Modulation. *Nat. Commun.* **2019**, *10*, 1391.

(58) Goldschmidt, J. C. *Novel Solar Cell Concepts*, University of Konstanz, 2009.

(59) Kuznetsov, S. V.; Alexandrov, A. A.; Fedorov, P. P. Optical Fluoride Nanoceramics. *Inorg. Mater.* **2021**, *57*, 555–578.

(60) Richards, B. S.; Hudry, D.; Busko, D.; Turshatov, A.; Howard, I. A. Photon Upconversion for Photovoltaics and Photocatalysis: A Critical Review. *Chem. Rev.* **2021**, *121*, 9165–9195.

(61) Hofmann, C. L. M.; Fischer, S.; Eriksen, E. H.; Bläsi, B.; Reitz, C.; Yazicioglu, D.; Howard, I. A.; Richards, B. S.; Goldschmidt, J. C. Experimental Validation of a Modeling Framework for Upconversion Enhancement in 1D Photonic Crystals. *Nat. Commun.* **2021**, *12*, 104.

(62) Das, A.; Mao, C.; Cho, S.; Kim, K.; Park, W. Over 1000 Fold Enhancement of Upconversion Luminescence Using Water Dispersible Metal Insulator Metal Nanostructures. *Nat. Commun.* **2018**, *9*, 4828.

(63) Liu, Q.; Liu, H.; Li, D.; Qiao, W.; Chen, G.; Ågren, H. Microlens Array Enhanced Upconversion Luminescence at Low Excitation Irradiance. *Nanoscale* **2019**, *11*, 14070–14078.